Key Engineering Materials
ISSN: 1662-9795, Vol. 926, pp 194-205
doi:10.4028/p-8134oi

Submitted: 2021-12-08
Accepted: 2022-02-18
Online: 2022-07-22

18Ni300 Maraging Steel Produced via Direct energy Deposition on H13 Tool Steel and DIN CK45

Jorge Gil[1,a*], Ricardo Seca[,2,b], Rui Amaral[,1,2,c], Omid Emadinia[,2,d], Ana Reis[,1,2,e], and Abílio de Jesus[1,2,f]

[1]Institute for Science and Innovation in Mechanical and Industrial Engineering, R. Dr. Roberto Frias 400, Porto 4200-465, Portugal

[2]Faculty of Engineering of the University of Porto, s/n, R. Dr. Roberto Frias, Porto 4200-465, Portugal

[a] jgil@inegi.up.pt, [b] rseca02@gmail.com, [c]ramaral@inegi.up.pt, [d]oemadinia@inegi.up.pt, [e] areis@inegi.up.pt, [f]ajesus@fe.up.pt

Keywords: Metallic Additive Manufacturing, Direct Energy Deposition, Maraging Steel

Abstract. The quality of metallic additive manufacturing outputs is heavily dependent on the employed processing parameters. Hence, the assessment and definition of the input variables appropriate to the material in question is of vital importance, in order to optimise the attainable properties and minimise wasted feed stock in failed trials.

In this work, optimal parameters for 18Ni300 Maraging steel are found for deposition in an H13 substrate. Additinally, the influence of pre-heating in depositions on a DIN CK45 steel are analysed by optical microscopy (OM) and microhardness measurements along the interface, and mechanical characterisation of DED-produced 18Ni300 is performed, as well as a bi-metallic alloy comprised of 18Ni300 and CK45, through the production and testing of tensile specimens.

Introduction

Additive manufacturing (AM) processes have recently witnessed a considerable increase in interest from production-related sectors, as these processes are capable of producing components free from most geometric constraints that are expected in conventional manufacturing processes [1]. A far-cry from their original purpose of producing prototypes to aid the design and visualisation process, AM methods are now capable of processing a vast array of materials - including metallic materials - and are used in the manufacture or repair of near-net shape structural components [2]. Direct energy deposition (DED) is a powder-based process that is specially useful in the repair of already existing components due to its high productivity when compared to its counterparts such as laser powder bed fusion (LPBF), and absence of a powder-bed, as the feedstock is ejected from a nozzle directly into a heat source [3]. DED has many aliases such as directed light fabrication (DLF), laser engineered net shaping (LENS), laser-based additive manufacturing (LBAM), among other acronyms, although the differences between these processes are minor when compared to their shared underlying technology: a powdered feedstock is ejected by a coaxial nozzle into a melting pool, originated by the interaction between the heat-source, the previously expelled powder and the substrate or component. The heat source is generally a laser, with most common lasers being either solid-state Nd:YAG or fibre lasers [3]. An inert gas is also ejected into the melting pool to avoid corrosion phenomena; a schematic representation of a generic DED process is shown in Figure 1.

Considering repairing operations as one of the largest advantages of DED, there is a large number of applications in which extending the life cycle of components proves very profitable and attractive; one example is the repair of casting dies, which are generally expensive and time-consuming to manufacture [4], requiring exceptional mechanical properties to temperatures up to 300 °C, resistance to abrasion and resistance to craze cracking induced by successive thermal shocks. One possible material used within this context are Maraging steels, more specifically 18Ni300, for several reasons: *(i)* Maraging steels are very printable alloys [5], dealing well with the multiple thermal cycles associated

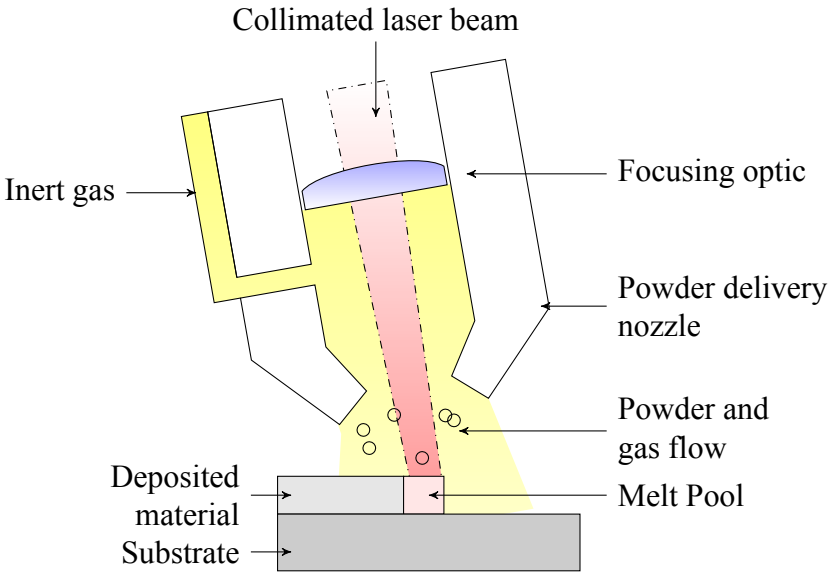

Fig. 1: Schematic representation of the direct energy deposition process.

with the printing process; *(ii)* it is a precipitation hardenable alloy, granting the possibility of reaching exceptional ($\geq$2000 MPa) yield strength and hardness; *(iii)* it is machinable, particularly so before precipitation hardening. The major disadvantage of Maraging alloys are their lack of corrosion resistance, although several products have been put forth to bridge this shortcoming [6]. Several studies have been performed regarding the process optimisation of AM-produced Maraging steels, although mainly focused in PBF processes: Ten et al (2017) concluded that grade 300 Maraging steels produced via AM could achieve wrought-level properties [7]; Kempen et al. (2011) optimised the heat treatment procedures, yielding samples with hardness of 58 HRC and a yield strength of 2216 MPa, at the cost of reduced elongation from 13% to 2% [8]; Martínez et al. (2020) optimised DED parameters in manufacturing 18Ni300 on a substrate of the same material for both cladding and three-dimensional geometry production [9]; Kürnsteiner et al. (2017) increased the hardness in 19% Maraging by increasing the Al content, leading to the precipitation of NiAl nanoparticles that increased hardness even in the absence of ageing [10]. In this work, DED-related parameter optimisation of 18Ni300 is performed on an H13 substrate, with the aim of studying the viability of DED-produced 18Ni300 as a repair solution in casting dies. AISI H13 is frequently used in injection dies due to its exceptional hot-working characteristics and corrosion resistance. Furthermore, the deposition on CK45 is conducted with and without the employment of pre-heating in order to analyse its influence in the microhardness and microstructures along the interface between the cladded surface and substrate, and a mechanical characterisation of DED-produced 18Ni300 is performed, along with a bi-metallic specimen comprised of 18Ni300 and DIN CK45, through tensile testing.

Materials and Methods

DED system. The used direct energy system is composed of a Coherent Highlight FL3000 fibre laser with a maximum power of 3000 W in continuous wave (CW) mode, presenting a wavelength of 1070+-10 nm. The powder is stored in two Medicoat AG Disk powder feeders, which deliver the feedstock to a Fraunhoffer powder splitter, in turn diverting the powder and gas flow into four orifices of a COAX12V6 nozzle head with a capacity of temperature regulation up to 6000 W. The robotic arm is a 6-axis KUKA industrial robot. The employed inert gas is Argon, fed by a cannister controlled by a pressure regulating valve set at 6 bar.

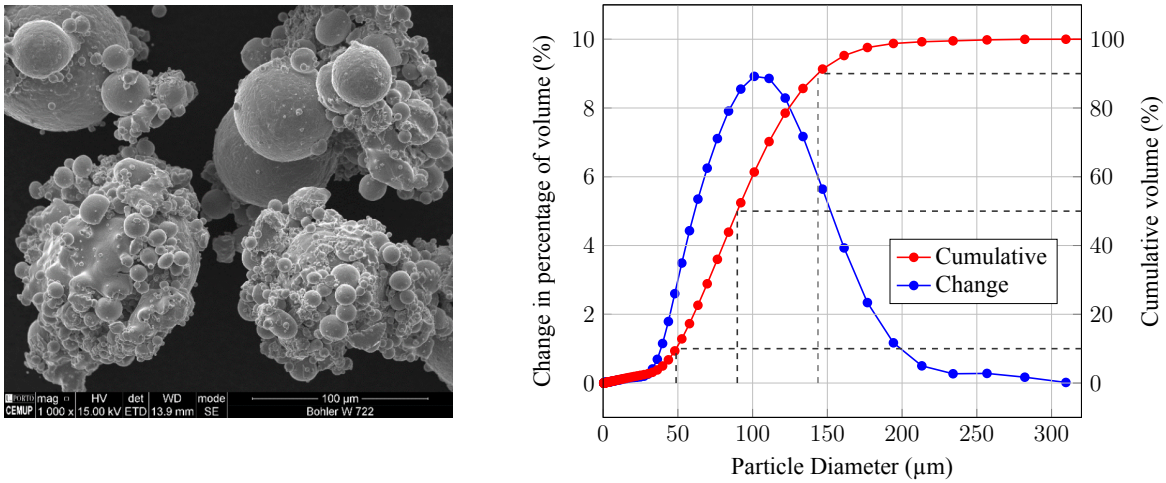

(a) Morphology. (b) Size distribution.

Fig. 2: Morphology and shape distribution of the W722 powder, used in the deposition.

Table 1: Shape distribution of the W722 powder, used in the deposition.

D_{10} [µm]	D_{50} [µm]	D_{90} [µm]
48.80	89.75	143.73

Powder and Substrate. The powdered feedstock was Böhler W722 (Böhler Edelstahl GMBH, Germany), an equivalent to the 18Ni300 Maraging steel grade, produced via inert gas atomisation [11]. Its shape, size and morphology was analysed through scanning electron microscopy (SEM), while the size distribution was determined through dynamic light scattering (DLS) by mixing the powder in an ethanol solution and ultrasonically vibrating the solution for one minute, with the aim of disassociating powder agglomerates. The powder's shape and morphology is shown in Figure 2a, while the size distribution is displayed in Figure 2b. The computed D_{10}, D_{50} and D_{90} diameters are shown in Table 1, with its values within the supplier's nominal guarantees.

The substrate was, as aforementioned, AISI H13 (FRamada, Portugal), annealed at $850\,°C$; its chemical composition was determined through optical emission spectroscopy (OES) in a SPECTROMAXx (Spectro). Its chemical composition is shown in Table 2.

Process Parameter Optimisation. Outputs produced via DED are heavily dependent on the employed parameters during manufacture; generally, three parameters are considered the most influential in the final build's quality [12]: *(i)* laser power, *(ii)* laser speed and *(iii)* feed rate. There are more parameters which impact the build quality, with varying degrees of flexibility and influence, such as the laser wavelength, beam energy distribution, laser spot diameter, powder carrier gas flow, shielding gas flow, nozzle relative angle, laser stand-off distance and pre-heating temperature.

Table 2: Chemical composition of AISI H13 used as the substrate.

	Chemical Composition [wt%]							
H13	Cr	Mo	Mn	P	C	Si	V	Fe
Nominal	4.80-5.50	1.20-1.50	0.25-0.50	≤ 0.03	0.35-0.42	0.80-1.20	0.85-1.15	Bal.
Measured	5.23	1.12	0.37	0.01	0.40	0.87	0.74	Bal.

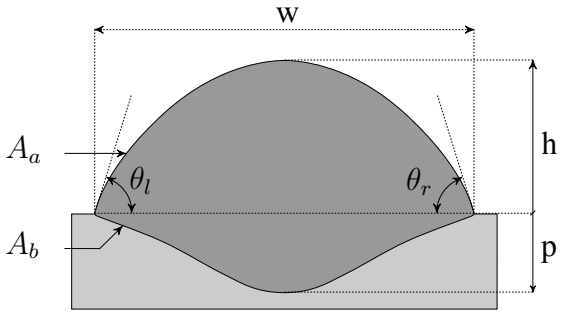

Fig. 3: Schematic representation of the cross-section of a DED-produced line bead and its associated parameters.

All depositions performed with the objective of optimising parameters were composed of 25 mm-long single tracks on H13, previously brushed and cleaned with acetone to diminish the presence of impurities and dust diluting with the deposited material. Initial evaluation was conducted through visual inspection, followed by cross-section analysis in optical microscopy (OM) of the line beads presenting very different input parameters, as a way to efficiently capture a significant sample size. With the OM imaging, several outputs were analysed, such as the clad width, height, penetration, wettability angles, area above the substrate, area below the substrate and dilution proportion. The latter is given by Equation (1)

$$D_{ap} = \frac{A_b}{A_b + A_a} \cdot 100\,[\%]\,. \tag{1}$$

in which A_a and A_b are the cross-section line bead area above and the cross-section area below the substrate. Figure 3 schematically shows the mentioned output variables.

Several criteria were adopted to evaluate the line bead's quality: *(i)* the optimal dilution window was set between 10% and 30% in accordance to literature [12][13]; *(ii)* the optimal wettability angles were established to be between $50°$ and $70°$, thus promoting good adhesion without excessive dilution nor increased probability of oxidation [3]; *(iii)* reduced presence or absence of pores, solidification cracks or other metallurgical defects.

Initial depositions followed an L9 Tagushi array between the laser power, laser speed and powder feeding rate. Multiple iterations were then performed, varying the remaining process parameters until an optimised line bead was produced. Two-dimensional parameters, such as the overlapping percentage between consecutive tracks, were optimised through 25×25 mm single layer depositions followed by section cutting and OM analysis.

Pre-heating influence. Four different 25×25 mm depositions with varying number of layers were conducted on CK45 substrates with the aim of studying the employment of pre-heating in the interface between the deposited material and the substrate (Table 3). The substrate's material was chosen with the objective of avoiding martensitic phase transformations through pre-heating above the martensitic start line of 380 °C. Optical microscopy (OM) imaging was obtained after sectioning and polishing the samples with 80, 180, 320 and 800 grit grinding discs (SiC Buehler CarbiMet) at 300 rpm in Struers Rotopol-21 polishing machines; polishing with an alumina suspension followed by grinding with diamond spray of 6 µm and 1 µm. Chemical etching was performed with Nital 10% during 15 s. Vickers microhardness measurements were taken with a Matsuzawa MXT70 machine, with a load of 100 gf for 15 s.

Preliminary tensile tests. Three specimens were manufactured and tested: *(i)* 100% 18Ni300, with the build direction perpendicular to the loading direction (these shall be henceforth named *horizontal*); *(ii)* 100% 18Ni300, with the build direction parallel to the loading direction (these shall henceforth

Table 3: Deposited samples for pre-heating study.

Specimen	Pre-heating Temperature [°C]	Number of Layers
A	-	1
B	-	3
C	400	1
D	400	3

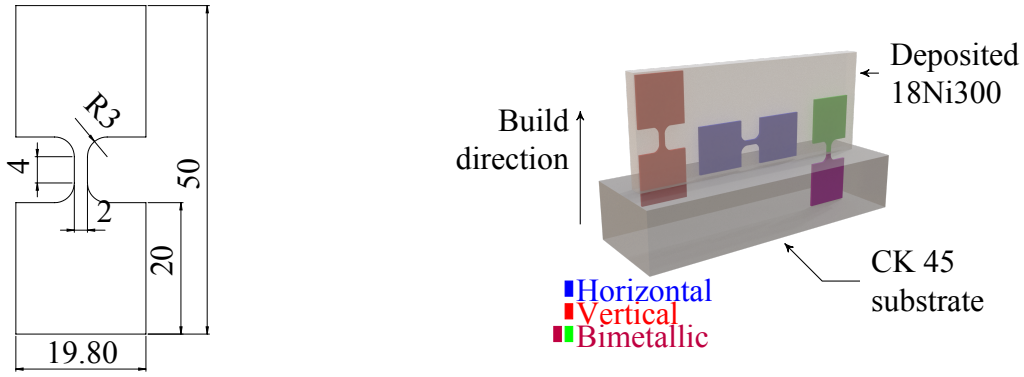

(a) Specimen geometry.

(b) Specimen extraction configuration.

Fig. 4: Miniaturized tensile test specimens extraction via wEDM from the deposited 18Ni300 steel.

be named *vertical*); *(iii)* 50% 18Ni300, 50% CK45, with the interface between both materials located in the testing section of the specimen (these shall be henceforth names *bi-metallic*). While the former specimens allow the mechanical characterisation of the deposited Maraging steel, the bimetallic specimen allows the characterisation of the adhesion between the deposited material and the substrate. The schematic representation of the specimen configuration is shown in Figure 4b.

The deposition from which the specimens were cut consisted on a $110 \times 6 \times 45$ mm geometry, with the parameters concluded to return the best result from the experiments in the H13 substrate, with these being: a ratio of laser power and laser spot size P/d_s of $740\,\mathrm{W\,mm^{-2}}$, a feeding rate f_r of $12\,\mathrm{g\,min^{-1}}$, scanning speed v_s of $12\,\mathrm{mm\,s^{-1}}$, carrier gas flow of $4\,\mathrm{L\,min^{-1}}$ and shielding gas flow of $30\,\mathrm{L\,min^{-1}}$. The specimens were then obtained through wire electrical discharge machining (wEDM). The specimen geometry is shown in Figure 4a and the schematic representation of the specimen configuration within the manufactured geometry is shown in Figure 4b. The tests were carried out in an Instron 5900R machine, with measurements carried out by Digital Image Correlation (DIC) at an acquisition rate of 10 Hz; given the uniform testing area, an average speckle size of less than 15 µm was employed. The used camera consisted of a 5 Megapixel BasleracA2440-75um, 2448x2048px with telecentric InfaimonOPE-TC-23-09,45mm lens. The commercial software for data post-processing was VIC-2D.v6, used to compute the strain field.

Results and Discussion

Parametrisation in H13. Initial depositions followed a L9 Tagushi array between the laser power, laser scanning speed and powder feeding rate. The carrier gas flow, shielding gas flow, spot size diameter, nozzle-to-substrate distance and nozzle angle remained constant throughout this initial trial, with values of $4.0\,\mathrm{L\,min^{-1}}$, $25.0\,\mathrm{L\,min^{-1}}$, 2.1 mm, 11.5 mm and 10°, respectively.

The large dilution proportion found in clad 1 encouraged the increase in the ratio between the scanning speed and the feeding rate; track 16 increased this input from 0.036 to 0.3, resulting in a decrease in dilution, although its wettability angles remained on pair with tracks 6 and 7, which feature ratios of 0.072 and 0.12, respectively. Track 32 and 35 improved the dilution proportion, with the latter

Table 4: Used parameters in the single track depositions pertaining to the parametrisation of 18Ni300 Maraging steel in an H13 substrate.

Track	Input Parameters						
	P [W]	v_s [mm s^{-1}]	f_r [g min^{-1}]	q_s [L min^{-1}]	q_c [L min^{-1}]	d_n [mm]	d_s [mm]
1	1250	3.0	5	25	4	11.5	2.1
2	1250	9.0	5	25	4	11.5	2.1
6	1500	9.0	10	25	4	11.5	2.1
7	1500	3.0	15	25	4	11.5	2.1
16	1400	6.0	12	25	4	11.5	2.1
32	1400	3.5	12	25	4	11.5	2.1
35	1400	12.0	12	25	4	11.5	2.1
50	1550	12.0	12	20	4	12.0	2.1
55	1550	12.0	12	25	3	13.0	2.1
56	1550	12.0	12	30	4	13.0	2.1

possessing wettability angles closer to the established optimal window, although the disparity between left and right angles is considerable; Alya et al. (2019) showed a relation between the nozzle angle and feeding rate when depositing on inclined surfaces, concluding that an increase in the mass flow rate generally increases the bead skewness at a fixed nozzle angle and laser power [14]. The laser power was subsequently increased to 1550 W, yielding a significant improvement in most metrics, albeit with a considerable dilution (31.12%) that was deemed appropriate. Within track 50's parameters of laser speed, laser power and feeding rate, trials were conducted by varying for the shielding gas, powder carrier gas and nozzle distance. The increase in shielding gas from 25 L min^{-1} to 30 L min^{-1} increased the disparity between wettability angles, with track 56 displaying $71°$ and $47°$ for the left θ_l and right θ_r wettability angles, respectively. This is likely due to increased turbulence in the melting pool. It is important to note, however, that this increase in disparity between angles may be offset by the benefits of increased protection against corrosion during deposition, a problem exacerbated in the processing in material without considerable anti-corrosion properties such as 18Ni300.

Table 5: Dimensional output analysis of single track depositions, used in selecting the optimised result.

Track	Output Parameters							
	w [mm]	h [mm]	p [mm]	θ_l [°]	θ_r [°]	A_a [mm^2]	A_b [mm^2]	D_p [%]
1	3.35	1.06	1.43	60.55	63.65	2.52	3.47	57.96
2	2.80	0.60	0.66	51.38	44.16	1.16	1.28	52.34
6	2.74	0.96	0.91	110.86	84.12	2.12	1.56	42.41
7	2.53	2.46	0.63	109.37	116.26	5.63	0.86	13.23
16	2.06	1.58	0.97	95.35	96.24	2.69	1.37	33.68
32	2.63	2.37	0.33	111.53	102.57	5.25	0.48	8.30
35	3.01	1.23	0.52	74.93	53.47	2.67	0.81	23.32
50	3.26	1.32	0.77	64.47	63.91	2.73	1.24	31.12
55	1.32	2.84	0.70	58.77	79.70	2.75	1.17	29.75
56	1.26	2.89	0.76	71.44	47.68	2.51	1.19	32.24

Complex parameters were established in order to achieve linear relations that allow the prediction of the bead's behaviour according to its input parameters. The physical significance of these parameters are, for the exception of the ratio between the feeding rate and scanning speed f_r/v_s, irrelevant

in the scope of the remaining work, and should be interpreted as mere numerical predictors, as they exemplify the complex relationship between the process variables and resulting outputs. The graphical representation of the acquired data is seen in Figures 5a-5d. Additionally, a parametrisation window was established, and is shown in both Figures 6a and 6b, with the latter being overlayed with the cross-sections of the deposited tracks. The processing map is based on V. Ocelík et. al. (2006) work on cobalt-based coatings on cast iron components [15], in which a optimal region for the clad's properties is established as a function of the wettabiity angles, dilution proportion and a minimum laser power setting. The optimal region for 18Ni300 Maraging steel is found to be at a ratio between the laser power and a laser diameter in the range of 700 and 800 W, a ratio of the scanning speed and feeding rate in the range of 0.05 and 0.06 m g^{-1}.

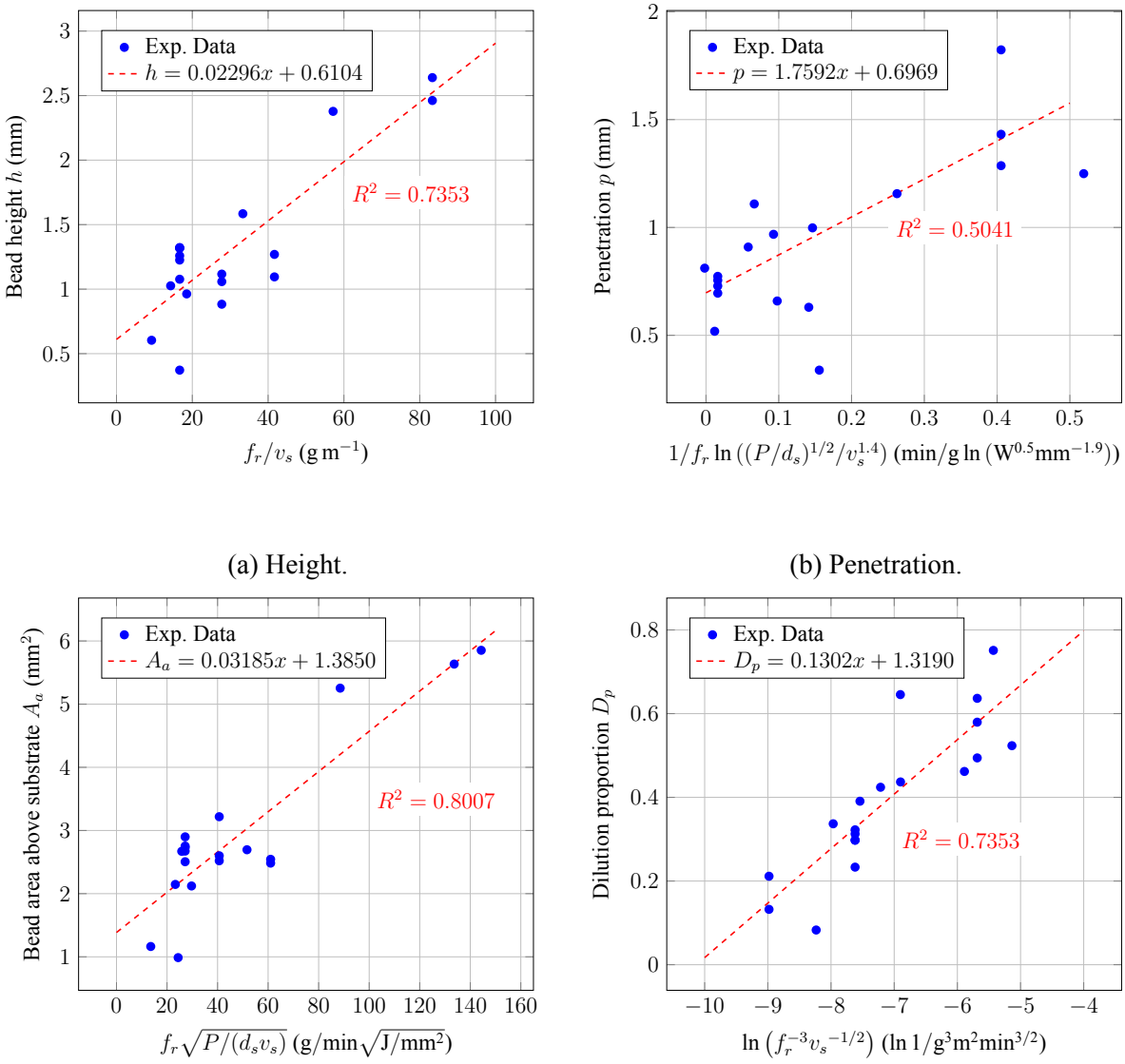

(a) Height.

(b) Penetration.

(c) Area above substrate.

(d) Dilution proportion.

Fig. 5: Best-fit linear regressions between different output variables and established complex parameters.

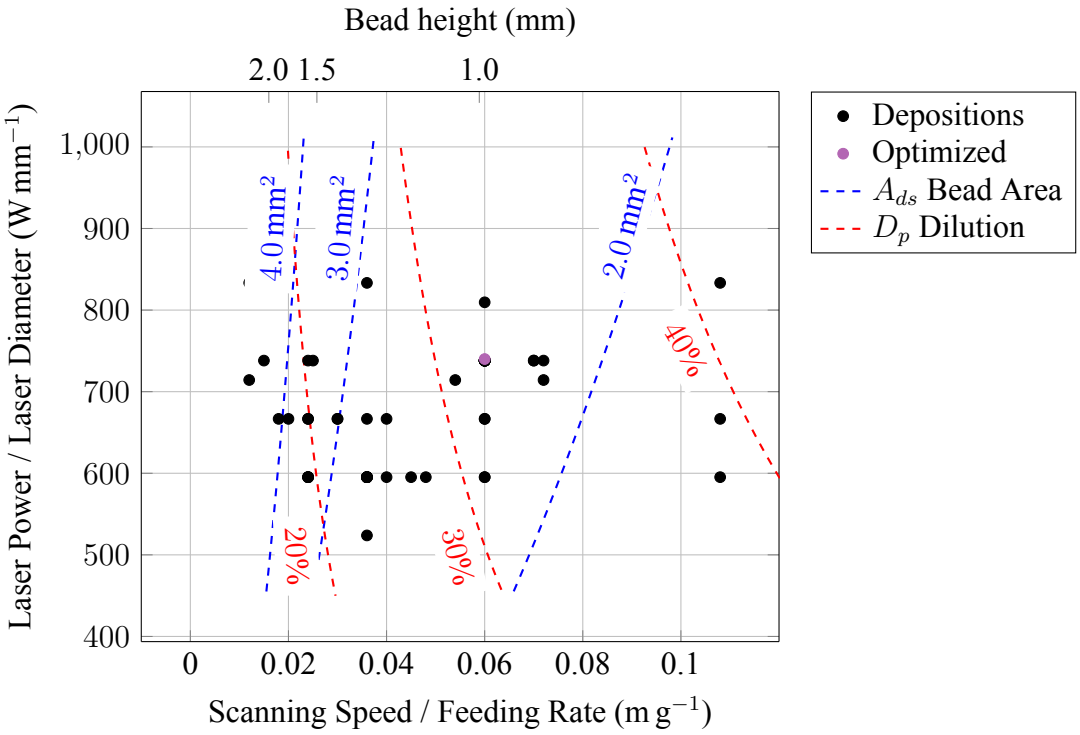

(a) Parametrisation window.

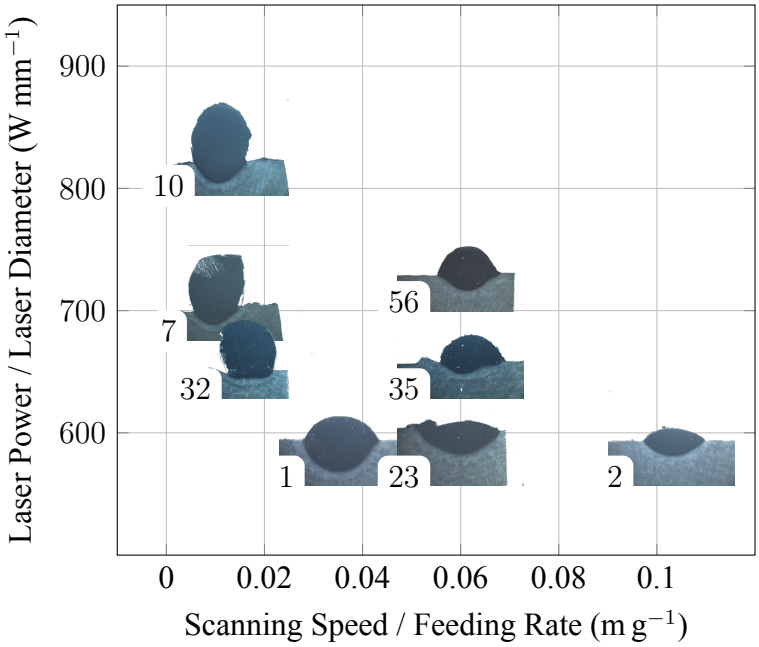

(b) Deposited tracks overlayed.

Fig. 6: Parametrisation window for DED-processed 18Ni300.

Pre-Heating Influence

OM imaging shows evidence of martensitic transformation near the interface between the cladded surface and the substrate, shown by the needle-like laths morphology indicated in Figure 7a. The non heat affected CK45 (Figure 7b) shows a perlitic and ferritic microstructure characteristic of this alloy. The microhardness measurements (Figure 7d) support this conclusion by displaying a clear spike to 702 HV near the interface, on CK45's side, for deposition A. Another important observation is made in deposition C, where the pre-heating appears to have prevented the formation of martensite, as the microhardness in the substrate's side of the interface is 227 HV. Additionally, the microhardness in the interface for sample B is of 225 HV, indicating that the deposition of additional layers and subjecting the already-deposited 18Ni300 to additional thermal cycles leads to a tempearing effect.

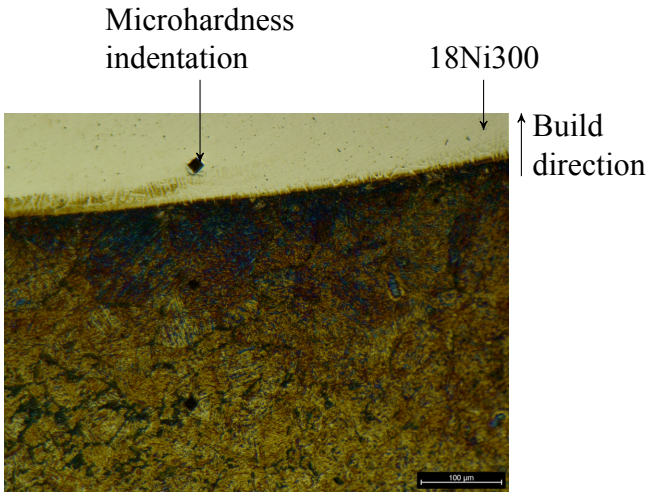

(a) Interface - sample A.

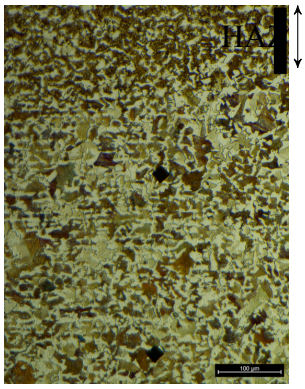

(b) Substrate - sample B.

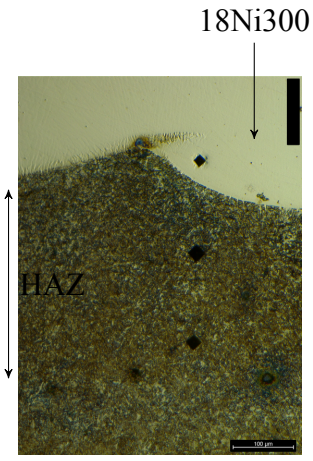

(c) Interface - sample B.

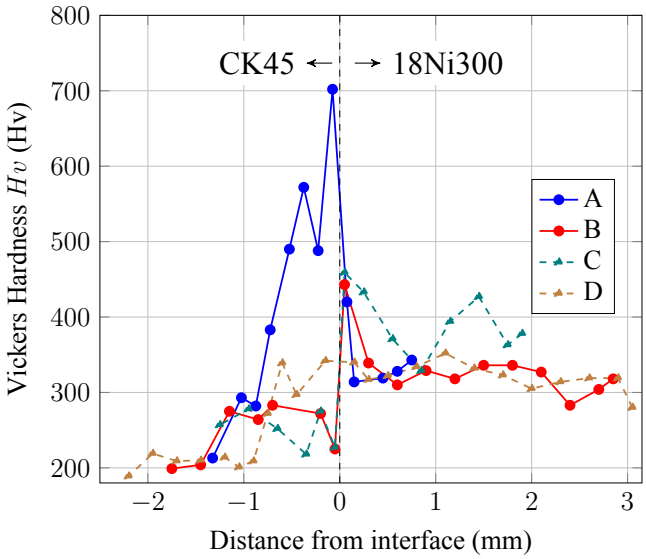

(d) Microhardness evolution.

Fig. 7: OM imaging obtained from samples A and B (7a-7c), and microhardness evolution along the interface between the substrate and cladded surface (7d).

Preliminary tensile tests. The results of the tensile tests carried out on the specimens entirely comprised of 18Ni300 are shown in Figure 8b-8a, for both directions. The results of the bimetallic specimens are shown in Figure . The vertical specimens displayed less plastic behaviour before rupture, a phenomena explained by the weaker adhesion between deposited layers. As material is deposited on top of the previously printed and solidified layers, the input energy must assure the melting of the ejected powder and the remelting of the already present material, increasing the probability of defects such as lack-of-fusion porosities arising. Regarding the yield strength S_y- shown in Table 6 alongside the ultimate tensile strength S_{uts} and the elongation at break e_b- its values are consistent with 18Ni30 before any heat treatment is undergone [16].

The bimetallic specimen fractured in the testing area comprised of CK45, with the interface region remaining intact, as seen in Figure 9b. Hence, the interface between both materials displays satisfactory adhesion. The force-displacement behaviour is shown in Figure 9a.

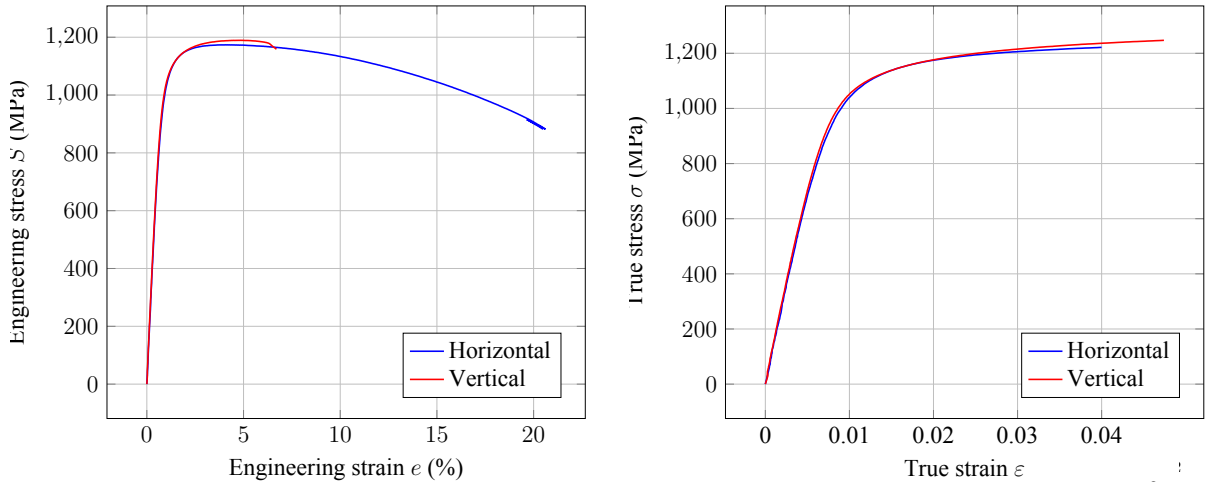

(a) Engineering stress-strain.

(b) True stress-strain.

Fig. 8: True stress-strain (7a) and engineering stress-strain (7b) curves from horizontal and vertical 100% 18Ni300 specimens.

Table 6: Mechanical properties of as-deposited 18Ni300 Maraging Steel, for vertical and horizontal specimens.

Specimen	S_y [MPa]	S_{uts} [MPa]	e_b [%]
Vertical	961.0	1189.4	6.7
Horizontal	955.7	1173.7	20.5

Conclusions

18Ni300 Maraging steel was successfully deposited in an H13 substrate, with parameters following ratio between the laser power and a laser diameter in the range of 700 and 800 W, a ratio of the scanning speed and feeding rate in the range of 0.05 and 0.06 m g^{-1}, a carrying gas flow of 4 L min^{-1} and a shielding gas flow of at least 25 L min^{-1}. Linear relations were established to predict parameter outputs from the systematic variables. The influence of the pre-heating temperature in the microhardness and microstructure was accounted for, with a pre-heating temperature above the martensite start temperature successfully preventing this phase transformation, with microhardness measurements differing between 702 HV and 227 HV for the pre-heated and non-pre-heated one layered geometry, respectively. However, it was seen that the deposition of multiple layers is sufficient to provoke a tempering

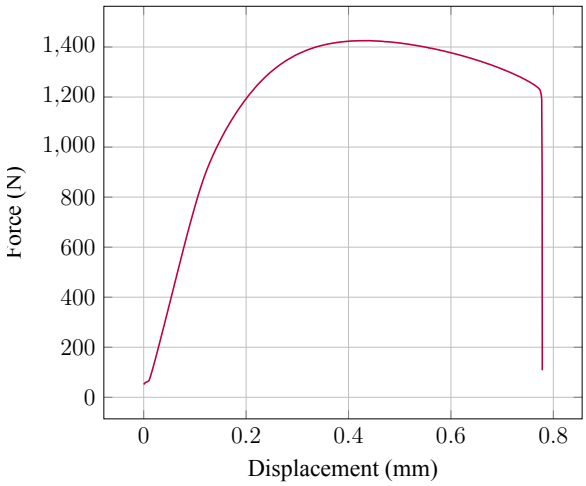

(a) Force-displacement curve.

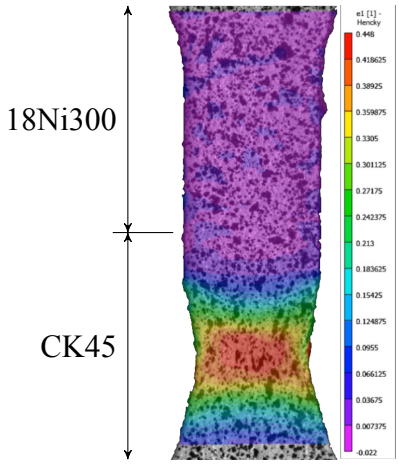

(b) DIC-computed strain field of bi-metallic specimen

Fig. 9: Force-displacement curve for bi-metallic specimen (9a) and DIC-computed strain field of bi-metallic specimen before rupture (9b).

effect on the CK45 substrate, rendering pre-heating inefficient in this particular situation as martensite is subjected to transformation and the hardness near the interface greatly decreases. The tensile specimens comprised of 100% 18Ni300 displayed similar yield and ultimate tensile strengths, with the main difference being the elongation at break, which was of 6.7 and 20.5 for the vertical and horizontal specimens, respectively. Thsi difference in ductility may be attributable to the weaker adhesion between different deposited layers. The bi-metallic specimen comprised of CK45 and 18Ni300 ruptured entirely within the substrate's region, implying a good adhesion between both materials.

Acknowledgments

The author acknowledges the funding of his PhD scholarship with the reference UI/BD/150684/2021 funded by FCT. The following projects are recognized and acknowledged: Add.Strength (PTDC/EME-EME/31307/2017), MAMTool (PTDC/EME-EME/31895/2017), ADDing (POCI-01-0145-FEDER-030490), Tooling (POCI-01-0247-FEDER-024516) and Add.Additive (POCI-01-0247-FEDER-024533), funded by FEDER funds and FCT.

References

[1] T. DebRoy, H. L. Wei, J. S. Zuback, T. Mukherjee, T. Elmer, J. O. Milewski, A. M. Beese, A. M. Wilson-Heid, W. Zhang. Additive Manufacturing of Metallic Components - Process, Structure and Properties. Progress in Materials Science Vol. 92 (2017), p. 112-224

[2] S. M. Thompson, L. Bian, N. Shamsaei, A. Yadollahi. An overview of Direct Laser Deposition for additive manufacturing: Part I: Transport phenomena, modeling and diagnostics. Additive Manufacturing Vol. 8 (2015), p.37-59

[3] E. Toyserkani, A. Khajepour, S. Corbin, in: *Laser Cladding*. Publications/CRC Press, Boca Raton (2005)

[4] P. Beeley, in: *Foundry Technology*, Publications/Butterworth-Heinemann, Oxford (2001)

[5] C. Turk, H. Zunko, C. Aumayr, H. Leitner, and M. Kapp. 2019. Advances in Maraging Steels for Additive Manufacturing. BHM Berg-und Hüttenmännische Monatshefte, Vol. 164(3) (2019), p. 112–116

[6] voestalpine BÖHLER Edelstahl GmbH & Co KG, BÖHLER M789 AMPO Product Data Sheet, 2018

[7] C. Tan, K. Zhou, W. Ma, P. Zhang, M. Liu, and T. Kuang. Microstructural evolution, nanoprecipitation behavior and mechanical properties of selective laser melted high-performance grade 300 maraging steel.Materials & Design Vol. 134 (2017), p. 23-34.

[8] K. Kempen, E. Yasa, L. Thijs, J. P. Kruth, J.K. Van Humbeeck. Microstructure and mechanical properties of Selective Laser Melted 18Ni-300 steel. Physics Procedia Vol. 12 (2011), p. 255-263

[9] C. Félix-Martinez, J. Ibarra-Medina, D. A. Fernández-Benavides, L.A. Cácerez-Díaz, J. M. Alvarado-Orozco. Effect of the parametric optimization and heat-treatment on the 18Ni-300 maraging steel microstructural properties manufactured by directed energy deposition. The International Journal of Advanced Manufacturing Technology Vol. 115 (2021), 3999-4020

[10] P. Kürnsteiner, M. Wilms, A. Weisheit, P. Barriobero-Vila, E. Jägle, D. Raabe. Massive nanoprecipitation in an Fe-19Ni-xAl maraging steel triggered by the intrinsic heat treatment during laser metal deposition Vol. 129 (2017), p.52-60

[11] voestalpine BÖHLER Edelstahl GmbH & Co KG, BÖHLER W722 AMPO Product Data Sheet, 2018

[12] Ferreira, A., Amaral, R., Romio, P., Cruz, J., Reis, A., Vieira, M., . Deposition of nickel-based superalloy claddings on low alloy structural steel by direct energy deposition, Metals Vol. 11(8) (2021), p. 1326

[13] A. Dass, A. Moridi, 2019. From additive manufacturing to materials design, Coatings Vol. 9(7) (2019), p. 1-26

[14] S. Alya, C. Vundru, B. Ankamreddy and R. K. Singh Characterization and modeling of deposition geometry in directed energy deposition over inclined surfaces. Procedia Manufacturing Vol. 34 (2019), p. 695-703

[15] V.Ocelík, U. de Oliveira, M.de Boer, J.Th.M.de Hosson. Thick Co-based coating on cast iron by side laser cladding: Analysis of processing conditions and coating properties. Surface and Coatings Technology Vol. 201(12) (2007), p. 5875-5883

[16] R. Fang, N. Deng, H. Zhang, G. Wang, Y. Su, H. Zhou, K. Gao, L. Gu. Effect of selective laser melting process parameters on the microstructure and properties of a precipitation hardening stainless steel. Materials & Design Vol. 212 (2021), p. 1-14